



# Magnetic, magnetocaloric properties, and critical behavior in a layered perovskite $\text{La}_{1.4}(\text{Sr}_{0.95}\text{Ca}_{0.05})_{1.6}\text{Mn}_2\text{O}_7$

Arwa Belkahlia<sup>1,\*</sup>, K. Cherif<sup>1</sup>, J. Dhahri<sup>1</sup>, and E. K. Hlil<sup>2</sup>

<sup>1</sup>Département de Physique, Faculté des Sciences de Monastir, Laboratoire de la matière condensée et des nanosciences, 5000 Monastir, Tunisia

<sup>2</sup>Institut Neel, CNRS et Université Joseph Fourier, BP 166, 38042 Grenoble, France

Received: 27 February 2016

Accepted: 6 May 2016

Published online:  
19 May 2016

© Springer Science+Business  
Media New York 2016

## ABSTRACT

We report the results of magnetic, magnetocaloric properties, and critical behavior investigation of the double-layered perovskite manganite  $\text{La}_{1.4}(\text{Sr}_{0.95}\text{Ca}_{0.05})_{1.6}\text{Mn}_2\text{O}_7$ . The compounds exhibits a paramagnetic (PM) to ferromagnetic (FM) transition at the Curie temperature  $T_C = 248$  K, a Neel transition at  $T_N = 180$  K, and a spin glass behavior below 150 K. To probe the magnetic interactions responsible for the magnetic transitions, we performed a critical exponent analysis in the vicinity of the FM–PM transition range. Magnetic entropy change ( $-\Delta S_M$ ) was estimated from isothermal magnetization data. The critical exponents  $\beta$  and  $\gamma$ , determined by analyzing the Arrott plots, are found to be  $T_C = 248$  K,  $\beta = 0.594$ ,  $\gamma = 1.048$ , and  $\delta = 2.764$ . These values for the critical exponents are close to the mean-field values. In order to estimate the spontaneous magnetization  $M_S(T)$  at a given temperature, we use a process based on the analysis, in the mean-field theory, of the magnetic entropy change ( $-\Delta S_M$ ) versus the magnetization data. An excellent agreement is found between the spontaneous magnetization determined from the entropy change [ $(-\Delta S_M)$  vs.  $M^2$ ] and the classical extrapolation from the Arrott curves ( $\mu_0 H/M$  vs.  $M^2$ ), thus confirming that the magnetic entropy is a valid approach to estimate the spontaneous magnetization in this system and in other compounds as well.

## Introduction

In recent years, the magnetocaloric effect (MCE) and electrocaloric effect (ECE) have become a promising technology because of their potential advantages over

the conventional gas compression refrigeration, particularly for low energy consumption, higher efficiency, low capital cost, and not using hazardous chemicals or global-warming gases [1–8]. The MCE is known to be one of the most interesting properties

Address correspondence to E-mail: arwabk123@gmail.com

and has been studied for the magnetic material with the aim of suppressing the emission of pollution components. It is an intrinsic to all magnetic materials and is due to the coupling of the atomic magnetic moments with the magnetic applied field which can produce a large entropy variation [9, 10]. So the purpose of using the MCE is to seek the proper material whose transition temperature is near room temperature of the magnetocaloric materials [11, 12]. The ECE, which is associated with the temperature dependence of the macroscopic polarization under an electric field, has been spasmodically studied in ferroelectric materials in order to find an alternative to classical refrigerators using Freon [13, 14].

In the past few years, many studies have revealed that double-layered perovskite manganite  $\text{RE}_{2-2x}\text{M}_{1+2x}\text{Mn}_2\text{O}_7$  (RE is a trivalent rare-earth cation like Pr, Nd or La, and M is a divalent alkaline earth cation like Ba, Sr, or Ca) are the ones the of most fascinating materials in the condensed matter research and exhibit intriguing features, like the notable colossal magnetoresistance (CMR) and magnetocaloric effect (MCE), due to their fascinating properties related to the ferromagnetic (FM)-paramagnetic (PM) transition [15–19]. The structure of the double-layered manganite is a stack of ferromagnetic metal sheets composed of  $\text{MnO}_2$  bilayers separated by a rock salt nonmagnetic insulating layer  $(\text{RE}, \text{M})_2\text{O}_2$ . Thus the RE and M ions are located in both the  $\text{MnO}_2$  bilayers and in the rock salt layer, and their distribution is dependent on the dopant ion size.

Many previous reports were dedicated that layered manganite has a rich phase diagram which had a strong dependence on magneto-transport properties. Basically, we still believe that the origin of the ferromagnetic (FM) phase and metallicity is related to the double-exchange (DE) interactions which implies a ferromagnetic pairing between  $\text{Mn}^{3+}(t_{2g}^3 \uparrow e_g^1 \uparrow, S = 2)$  and  $\text{Mn}^{4+}(t_{2g}^3 \uparrow e_g^0, S = 3/2)$  ions and antiferromagnetic (AFM) super-exchange (SE) interactions of  $\text{Mn}^{3+}-\text{O}^{2-}-\text{Mn}^{3+}$  and  $\text{Mn}^{4+}-\text{O}^{2-}-\text{Mn}^{4+}$  pairs [20, 21]. In the DE interaction, the electron hops from  $\text{Mn}^{3+}$  to  $\text{O}^{2-}$ , accompanied by a simultaneous hop from the latter to  $\text{Mn}^{4+}$ . The probability of this DE electron transfer of an e.g., electron depends on the orientation of the neighboring intra-atomic Hund coupled  $t_{2g}$  spins. The probability of hopping is also strongly dependent on the structural parameters such as Mn–O–Mn bond angle and  $\text{Mn}^{3+}$ ,  $\text{Mn}^{4+}$  concentrations.

However, metallicity and ferromagnetism are well explained by the DE interaction, which could not adequately explain the paramagnetic insulating phase occurring at high temperature. The presence of a paramagnetic phase is explained by the concept that the mobile electron carries with it the Jahn–Teller distortion of the  $\text{MnO}_6$  octahedron [22]. The greater distortion results in more localized charge carriers. This deformation disappears in the metallic state below the ferromagnetic transition.

To get a clear idea about the performance of materials used in magnetic refrigeration devices, it is necessary to understand how their MCE evolves in desired temperature and magnetic field ranges. A detailed analysis of  $\Delta S_M(T, \Delta H)$  data provides the important information about magnetocaloric properties of materials. Recently, the MCE in  $\text{La}_{2-2x}\text{Sr}_{1+2x}\text{Mn}_2\text{O}_7$  compounds has been studied upon the magnetic entropy change ( $\Delta S_M$ ) [23, 24]. Also, these materials exhibit large ( $\Delta S_M$ ) under a moderate magnetic field [25–28]. High ( $\Delta S_M$ ) at low magnetic field changes and tunable magnetic phase transition properties make these materials good candidates as working elements in magnetic refrigeration applications.

In this work, we present a detailed of the magnetic, magnetocaloric effect, and critical behavior for  $\text{La}_{1.4}(\text{Sr}_{0.95}\text{Ca}_{0.05})_{1.6}\text{Mn}_2\text{O}_7$  polycrystalline sample. We have also used the phenomenological model to predict the values of the magnetocaloric properties (such as relative cooling power (RCP), heat capacity change, and entropy change) from calculation of magnetization as a function of temperature under different external magnetic fields.

## Experiment

Polycrystalline  $\text{La}_{1.4}(\text{Sr}_{0.95}\text{Ca}_{0.05})_{1.6}\text{Mn}_2\text{O}_7$  was synthesized by the sol–gel method using metal nitrates as starting materials [29]. Identification of the crystalline phase and structural analysis were carried out using “PANalytical X’Pert Pro” diffractometer with filtered (Ni filter) Cu radiation ( $\lambda_{\text{Cu } K\alpha 1} = 1.54056 \text{ \AA}$ ). The data were analyzed by the Rietveld method.

The magnetization and susceptibility measurements versus temperature ( $T$ ) and versus magnetic field ( $\mu_0 H$ ) were made by BS2 magnetometers developed in Louis Neel Laboratory at Grenoble. The

DC magnetic properties were carried out in both zero-field-cooled (ZFC) and field-cooled (FC) modes over a temperature range of 5–300 K with an applied magnetic field of 0.05 T. The isothermal  $M(\mu_0H)$  data were measured under a magnetic field varying from 0 to 5 T at several temperatures ( $T$ ).

## Results and discussion

### Structural characterization

Identification of the phase and structural analysis by X-ray diffraction were reported elsewhere [29]. The Rietveld refinement at room temperature revealed the presence of single phase with a tetragonal structure (I4/mmm). The lattice parameters of the perovskite phase are  $a = b = 3.8714 \text{ \AA}$ ,  $c = 19.3267 \text{ \AA}$ , and a cell volume of  $289.66 \text{ \AA}^3$ .

Figure 1 shows the unit cell structure of tetragonal double perovskites.

### Magnetic properties

Temperature dependence of the magnetization  $M(T)$  in zero-field-cooling (ZFC) and field-cooling (FC) modes recorded in the temperature range of 5–300 K under a magnetic field of 0.05 T are presented in Fig. 2.

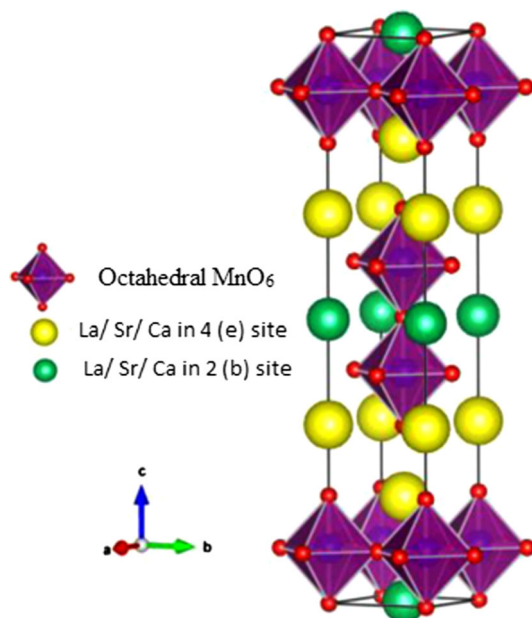


**Figure 1** The unit cell structure of tetragonal double perovskites.

The  $M(T)$  curves clearly indicate that  $\text{La}_{1.4}(\text{Sr}_{0.95}\text{Ca}_{0.05})_{1.6}\text{Mn}_2\text{O}_7$  passes through three magnetic transitions: the first one is a sharp transition at higher temperatures resembling a paramagnetic (PM) to ferromagnetic (FM) transition where the Curie temperature  $T_C$ , is obtained from the inflexion point of  $dM/dT$  versus  $T$  curve, is found to be 248 K (inset of Fig. 2). This value is in accordance with those reported in the literature [28, 30].

The other one at  $T_N = 180 \text{ K}$  which has been attributed to an antiferromagnetic Neel transition, and a distinct divergence of field-cooled (FC) and zero-field-cooled (ZFC) magnetization was observed below 150 K. This is also ascribed to the existence of the spin glass (SG) behavior present in this double-layered manganite phase. Similar behavior was reported in some other double-layered manganite [31]. This irreversibility arises possibly due to the canted nature of the spins or due to the random freezing of spins as observed in systems with FM cluster embedded in AFM matrix [32, 33]. In detail, in the absence of the applied field, the bilayers are stacked antiferromagnetically while within them the manganese moments are arranged ferromagnetically. However, when the magnetic field is applied, these moments remain ferromagnetically ordered (in spite of the rotation through  $90^\circ$  from the zero-field direction), whereas the bilayers are stacked ferromagnetically and therefore the FM order is restored [34]. The spin glass state can be attributed to the

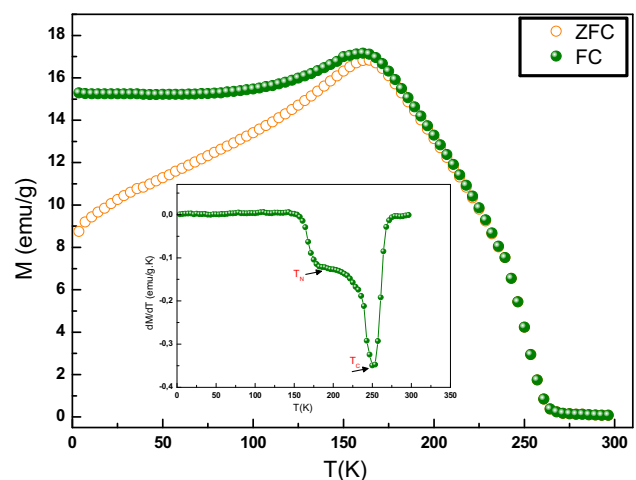


**Figure 2** Temperature dependence of FC and ZFC magnetizations for  $\text{La}_{1.4}(\text{Sr}_{0.95}\text{Ca}_{0.05})_{1.6}\text{Mn}_2\text{O}_7$  sample measured under low magnetic field of 0.05 T. *Inset* shows the magnetization derivate as a function of temperature curve for determining  $T_C$ .

coexistence of random competing ferromagnetic (FM) double-exchange involving the itinerant e.g., electrons and antiferromagnetic (AFM) super-exchange involving localized  $t_{2g}$  electrons together with the anisotropy originating from the layered structure [35]. In fact, the substitution of divalent ions ( $\text{Sr}^{2+}$  and  $\text{Ca}^{2+}$ ) for trivalent rare-earth ions ( $\text{La}^{3+}$ ) introduces excess electrons in the lattice. The excess electrons in the compounds enable the coexistence of  $\text{Mn}^{3+}$  and  $\text{Mn}^{4+}$  ions; as a result, the (FM) double-exchange interaction overcomes the inherent (AFM) super-exchange interaction. Furthermore, the electron in the itinerant e.g., state in  $\text{Mn}^{4+}$  increases the Mn–O orbital overlap, which increases the size of the super-exchange interaction and favors an antiferromagnetic state. Consequently, this competition between the super-exchange and double-exchange present in  $\text{La}_{1.4}(\text{Sr}_{0.95}\text{Ca}_{0.05})_{1.6}\text{Mn}_2\text{O}_7$  gives rise to the spin glass behavior [33, 36].

Figure 3 shows the temperature dependence of the inverse magnetic susceptibility  $\chi^{-1}$  deduced from  $M(T)$  curve. Above  $T_C$ , a sharp transition with a linear relation was observed and below  $T_C$  a clear deviation can be attributed to the antiferromagnetic transition (inset of Fig. 3).

In the paramagnetic region (above  $T_C$ ), the susceptibility obeys the Curie–Weiss law:

$$\chi = \frac{C}{T - \theta_{\text{CW}}}$$

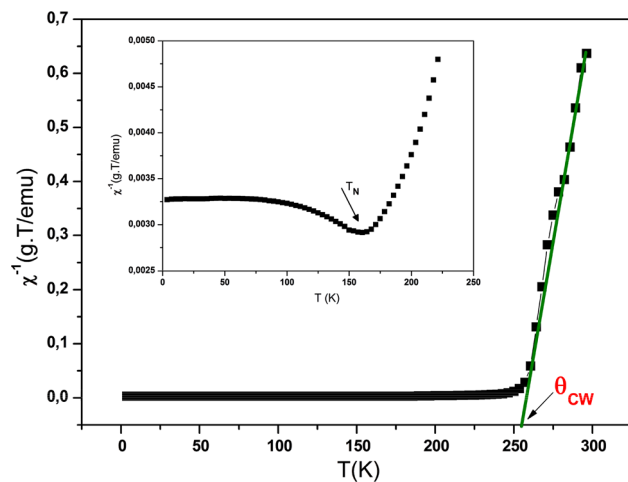


**Figure 3** Variation of the inverse of the magnetic susceptibility as a function of temperature for. The red solid line is the best fit using Curie–Weiss law in the paramagnetic range ( $T > T_C$ ). Inset shows a zoom of the antiferromagnetic transition.

where

- $\theta_{\text{CW}}$  is the Curie–Weiss temperature.
- $C$  is the Curie constant defined as:

$$C = \left( \frac{N_a}{3k_B M_m} \right) \mu_{\text{eff}}^{\text{exp}2}$$

With  $N_a$  is Avogadro number,  $M_m$  is the molecular mass per unit formula,  $k_B$  is Boltzmann constant, and  $\mu_{\text{eff}}^{\text{exp}}$  is the experimental effective moment expressed in Bohr magneton.

From the linear fit of the paramagnetic part ( $T > T_C$ ), we determined the values of  $\theta_{\text{CW}}$  and  $C$  which are, respectively, the intercept of the line with the temperature axis ( $\theta_{\text{CW}} = 252 \text{ K}$ ) and the inverse of the slope of the straight line ( $C = 63.13 \text{ emu. K/g T}$ ). The positive value of  $\theta_{\text{CW}}$  indicates the ferromagnetic interaction between spins.

The theoretical paramagnetic effective moment should be

$$\mu_{\text{eff}}^{\text{th}} = \sqrt{x\mu_{\text{eff}}^2(\text{Mn}^{3+}) + y\mu_{\text{eff}}^2(\text{Mn}^{4+})} \tag{1}$$

here  $\mu_{\text{eff}}^{\text{th}}(\text{Mn}^{3+}) = 4.9 \mu_B$ ,  $\mu_{\text{eff}}^{\text{th}}(\text{Mn}^{4+}) = 3.87 \mu_B$  and  $x = 0.7$ ,  $y = 0.3$  were determined using the same reasoning as Zhou et al. [37] (The ratio of  $\text{Mn}^{3+}$  to  $\text{Mn}^{4+}$  is the same for  $\text{La}_{1.4}(\text{Sr}_{0.95}\text{Ca}_{0.05})_{1.6}\text{Mn}_2\text{O}_7$  and  $\text{La}_{0.7}(\text{SrCa})_{0.3}\text{MnO}_3$ ).

It can be deduced that the experimental effective moment ( $\mu_{\text{eff}}^{\text{exp}} = 6.24 \mu_B$ ) is slightly larger than the expected theoretical value ( $\mu_{\text{eff}}^{\text{th}} = 4.61 \mu_B$ ) and the value obtained for  $\theta_{\text{CW}}$  is higher than that of  $T_C$ . This difference confirms the presence of a magnetic inhomogeneity resulting in short range ordered slightly above  $T_C$ .

For an accurate description of the low temperature behavior of magnetic properties and in order to calculate the exchange constant  $J_{\text{exc}}$ , the spin wave theory can be used. In the case of long wavelength, the temperature dependence of the magnetization is given by [38].

$$M(T, \mu_0 H) = M(0, \mu_0 H) * (1 - BT^{3/2} - CT^{5/2}), \tag{2}$$

where  $M(0, \mu_0 H)$  and  $M(T, \mu_0 H)$  are the saturation magnetization values at 0 K and T K, respectively;  $B$  and  $C$  are the characteristic constants of the long wavelength spin wave at low temperature. However, for a bulk ferromagnetic system, the temperature thermal evolution of magnetization  $M$  below the Curie temperature follows Bloch’s  $T^{3/2}$  law of the form [39].

$$M(T, \mu_0 H) = M(0, \mu_0 H) * (1 - BT^{3/2}), \quad (3)$$

where the pre-factor  $B$  is the Bloch constant of the spin waves that depends on the structure of the material and was obtained by fitting Eq. (3) to the experimental magnetization curves (Fig. 4) at low temperature range. This coefficient is given by the following relation [40].

$$B = 2.612 \left( \frac{g\mu_B}{M(0)} \right) * \left( \frac{k_B}{4\pi D} \right)^{3/2}. \quad (4)$$

In this expression,  $k_B$  is the Boltzmann constant,  $g$  is the Lande factor ( $g = 2$ ),  $\mu_B$  is the Bohr magnetron, and  $D$  is the spin wave stiffness constant.

This stiffness  $D$  is defined by spin wave dispersion relation [41]:

$$E(q) = \Delta + Dq^2. \quad (5)$$

The above relation is valid for  $q \rightarrow 0$ . Here,  $q$  is the momentum wave vector,  $\Delta$  is the gap arising from anisotropy or applied magnetic field  $\mu_0 H$ , and  $E$  is the spin wave energy. In our analysis we assume  $\Delta = 0$ .

Figure 4 shows the reduced magnetization  $M(T, \mu_0 H)/M(0, \mu_0 H)$  as a function of  $T^{3/2}$  for  $\mu_0 H = 0.05$  T.

Where  $M(0, \mu_0 H)$  was obtained by extrapolating  $M(T, \mu_0 H)$  curves to  $T = 0$  using a second-order polynomial. From this figure, we determine the spin-stiffness constant  $D$  according to the value of  $B$  which is the slope of the linear fit of this curve. The  $B$  and  $D$  values are listed in Table 1 and are in an excellent

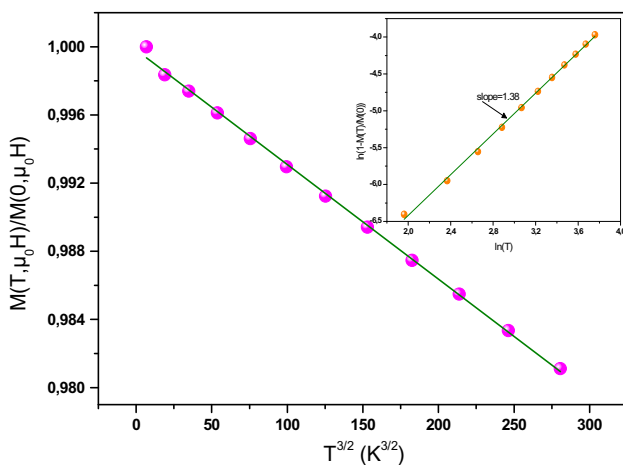


**Figure 4** Plot of  $M(T, \mu_0 H)/M(0, \mu_0 H)$  versus  $T^{3/2}$  for  $\text{La}_{1.4}(\text{Sr}_{0.95}\text{Ca}_{0.05})_{1.6}\text{Mn}_2\text{O}_7$ . The inset represents the variation of  $\text{Ln}[1 - M(T, \mu_0 H)/M(0, \mu_0 H)]$  versus  $\text{Ln}(T)$  in order to determine the slope.

agreement with those reported for other manganite [42].

The inset of Fig. 4 shows the curve  $\text{Ln}(1 - M(T, \mu_0 H)/M(0, \mu_0 H))$  versus  $\text{Ln}(T)$  which is used to verify that our compound obey Bloch's  $T^{3/2}$ . In this theory, the slope of the linear fit of this curve must be close to  $3/2$ . In our sample, we found that the slope is 1.38; therefore, we must note that Bloch's  $T^{3/2}$  law is valid for  $T < 100$  K.

The factor  $D$  is closely related to the degree of ferromagnetic exchange interaction ( $J_{\text{exc}}$ ) as given in Eq. (6).

$$J_{\text{exc}} = \frac{M(0)D}{2g\mu_B}. \quad (6)$$

The obtained parameter  $J_{\text{exc}}$  is listed in Table 1.

On the other hand,  $D$  and the Curie temperature  $T_C$  are linked by the following equation according to the Heisenberg model.

$$D = \frac{k_B r_{ij}^2 T_C}{2(S_{\text{Mn}} + 1)}, \quad (7)$$

where  $r_{ij}$  is the distance between nearest magnetic atoms (Mn) and  $S_{\text{Mn}}$  is the average spin moment between  $\text{Mn}^{3+}$  and  $\text{Mn}^{4+}$  atoms:

$$S_{\text{Mn}} = x_{\text{Mn}^{3+}} S(\text{Mn}^{3+}) + y_{\text{Mn}^{4+}} S(\text{Mn}^{4+}) \quad \text{Here } S(\text{Mn}^{3+}) = 2; S(\text{Mn}^{4+}) = \frac{3}{2}$$

Katsuki and Wollfarth [43] have discussed the correlation between  $D$  and the  $T_C$  on the basis of itinerant electron model. Using the effective mass approximation, they have obtained the following relationship:

$$D = \frac{\pi k_B T_C}{6\sqrt{2}k_F^2}, \quad (8)$$

where  $k_F$  is the Fermi wave vector obtained in Table 1.

Magnetization as a function of applied magnetic field  $M(\mu_0 H)$  of  $\text{La}_{1.4}(\text{Sr}_{0.95}\text{Ca}_{0.05})_{1.6}\text{Mn}_2\text{O}_7$  has been performed at 5 K in magnetic fields strengths of the range of  $\pm 10$  T and is displayed in the inset of Fig. 5.

**Table 1** Some magnetic parameter for  $\text{La}_{1.4}(\text{Sr}_{0.95}\text{Ca}_{0.05})_{1.6}\text{Mn}_2\text{O}_7$  compound

$B$ ( $10^{-5}$ $\text{K}^{-3/2}$ )	$D$ (meV $\text{\AA}^2$ )	$J_{\text{exc}}$ ( $10^{-23}$ J)	$r_{ij}$ ( $\text{\AA}$ )	$k_F$ ( $\text{\AA}^{-1}$ )
6.72	89	5	4.87	0.24

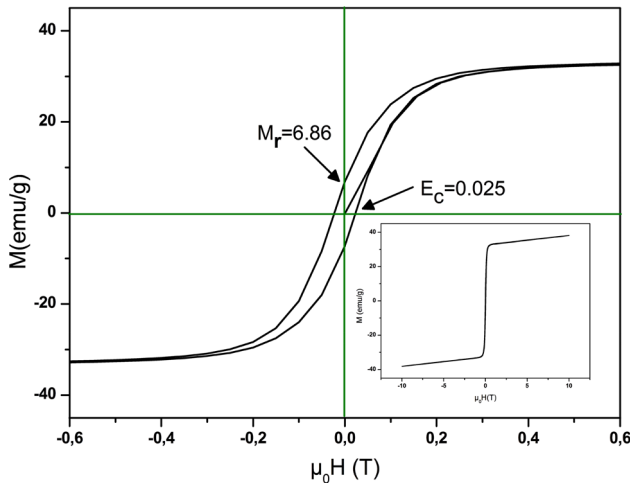


**Figure 5** The magnetic hysteresis loops at 5 K of the  $\text{La}_{1.4}(\text{Sr}_{0.95}\text{Ca}_{0.05})_{1.6}\text{Mn}_2\text{O}_7$  compound. The inset shows a zoom of the hysteresis loops at low field.

The Fig. 5 represents a zoom of the hysteresis loop at a low field and moderate values of the remanent magnetization and the coercive field. Clear hysteresis loops was observed in these curves and it can be seen that the magnetization increases sharply with the applied field for  $\mu_0H < 0.4$  T indicating the presence of a ferromagnetic state. After that, this magnetization increases almost linearly with increasing field value due to the presence of spin glass behavior. This phenomenon is based on the competition of AFM domains with FM ones. The magnetic hysteresis loop is not saturated at 5 T due to antiferromagnetic matrix.

Figure 6 represents the magnetization isotherms  $M(\mu_0H)$  registered in magnetic fields up to 5 T in the temperature range from 152 to 287 K at a temperature increment of  $\Delta T = 3$  K. These curves show that the magnetization increases sharply at low temperature in weak fields and then rises gradually with increasing field. However, when the temperature increases, the magnetization decreases and at Curie temperature, the sample transits from ferromagnetic to paramagnetic. This is because as temperature increases, originally magnetic ordered tends to clutter and disorder, magnetic momentum deflection occurs and hence the decrease in the total magnetic moment of the entire system, the magnetization of the sample decreases; when the temperature reaches near the Curie temperature, the thermal motion of the molecular of the material overcomes the ordered spin at zero-field, paramagnetism appears instead of

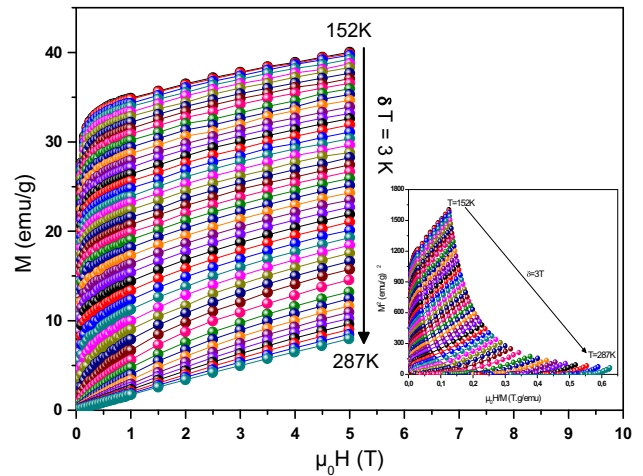


**Figure 6** Magnetization  $M$  versus magnetic applied field ( $\mu_0H$ ) at different temperatures. The inset is Arrott curves ( $M^2$  versus  $\mu_0H/M$ ) isotherms.

ferromagnetism. From this figure, no sign of saturation can be shown even at 5 T.

We draw in inset of Fig. 6 the Arrott plots  $M^2$  versus  $\mu_0H/M$  isotherms to define the order of the magnetic phase transition. This order can be determined from the slope from this figure according to the criterion given by Banerjee [44]. A positive or negative sign of the slope corresponds to a second- or first-order magnetic phase transition. For our sample, we can see clearly that the curve indicates positive slope in the high-field regions, indicating that the FM–PM transition is of a second order.

### Magnetocaloric study

The isothermal magnetization curve was used to calculate the magnetic entropy change ( $-\Delta S_M$ ), which is associated with the magnetocaloric effect, under the influence of a magnetic field.

From the Maxwell relations [45] based on the thermodynamical theory, the magnetic entropy change, induced by changing the magnetic field from 0 to  $\mu_0H$ , can be evaluated from the temperature using a numerical approximation as follows:

$$\begin{aligned} \Delta S_M(\mu_0H, T) &= S_M(\mu_0H, T) - S_M(0, T) \\ &= \int_0^{\mu_0H_{\max}} \left( \frac{\partial M(\mu_0H, T)}{\partial T} \right)_{\mu_0H} d(\mu_0H), \quad (9) \end{aligned}$$

where  $\mu_0H$  is the magnetic field,  $T$  is the temperature, and  $\mu_0H_{\max}$  is the maximum of the magnetic field. In

the case of magnetization measurements at small discrete magnetic field and temperature intervals,  $\Delta S_M$  can be approximated as

$$\Delta S_M \left( \frac{T_1 + T_2}{2} \right) = \frac{1}{T_1 - T_2} \left[ \int_0^{\mu_0 H_{\max}} M(T_2, \mu_0 H) \mu_0 dH - \int_0^{\mu_0 H_{\max}} M(T_1, \mu_0 H) \mu_0 dH \right] \quad (10)$$

According to Eq. (10), the magnetic entropy change for the sample as a function of temperature at various external magnetic fields is given in Fig. 7.

We can also observe two distinct maxima at 180 and 248 K: The lowest one is around Neel transition ( $T_N = 180$  K). In general, in simple perovskite around this transition ( $-\Delta S_M$ ) is negative [46], while in the double layered, we find that this ( $-\Delta S_M$ ) can be positive [47]. It is comparable with our results. The second is around the Curie temperature ( $T_C = 248$  K). In this temperature, ( $-\Delta S_M$ ) increases from 0.56 to 1.71 J kg<sup>-1</sup> K<sup>-1</sup> with increasing magnetic field (0.5–5 T), and the peaks are symmetrical enlargement and remain nearly unaffected. This phenomenon is in general characteristic of a second-order magnetic transition [48].

An important parameter used to estimate the magnetic cooling efficiency of our magnetocaloric material is the relative cooling power (RCP). This factor corresponds to the amount of heat per

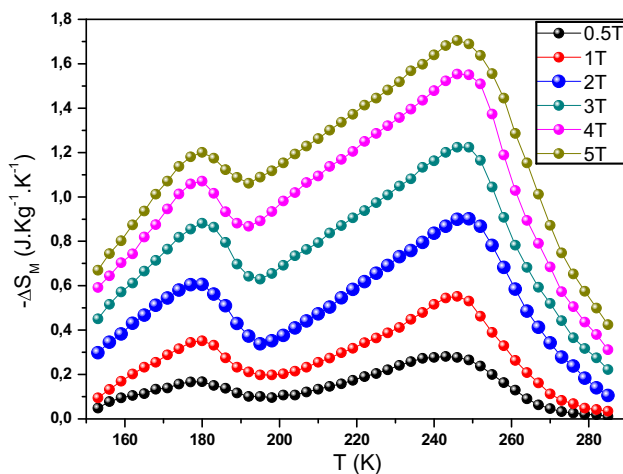


**Figure 7** Temperature dependence of the magnetic entropy change in various magnetic fields up to 5 T for samples.

kilogram that can be transferred between the cold and hot tanks during an ideal refrigeration cycle and is defined as [1]

$$RCP = -\Delta S_{\max} \times \delta T_{FWHM}, \quad (11)$$

where  $\Delta S_{\max}$  is the maximum magnetic entropy change, and ( $\delta T_{FWHM} = T_{\text{hot}} - T_{\text{cold}}$ ) is the full width at half maximum of the magnetic entropy change curve.

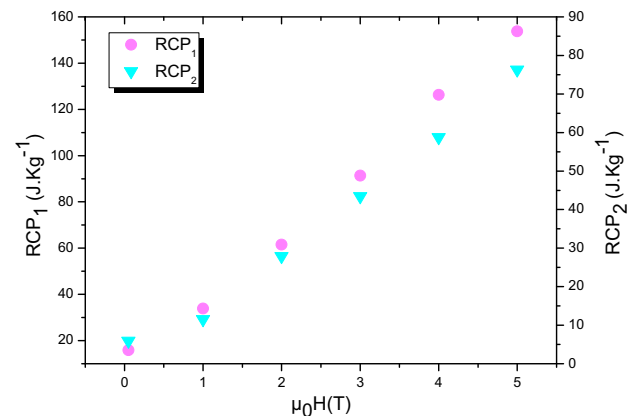
The relative cooling power has been calculated for both cases near  $T_C$  and around  $T_N$  and are noted, respectively,  $RCP_1$  and  $RCP_2$ .

Figure 8 shows the magnetic field dependence of RCP around  $T_C$  and  $T_N$ . From this figure, we can see that for both temperatures, the values of RCP increase with  $\mu_0 H$ . However, RCP around  $T_C$  is significantly more important than  $T_N$ . So a material in the same refrigeration cycle with higher RCP is preferred because it would confirm the transport of a greater amount of heat in an ideal refrigeration cycle [49].

The values of  $\Delta S_{\max}$  and  $RCP_1$  for the sample are summarized in Table 2, together with reported values of other materials for comparison.

The value  $RCP_1$  is considerable and comparable with those reported in the literature, and the magnetic entropy peak is broadening; these factors make this sample a promising candidate for magnetic refrigeration applications.

The change of specific heat ( $\Delta C_p$ ) associated with a magnetic field variation from 0 to  $\mu_0 H$  is given by [51–53].



**Figure 8** Magnetic field ( $\mu_0 H$ ) dependence of the  $RCP_1$  and  $RCP_2$  in both transitions.

**Table 2** Method of preparation, Curie temperature ( $T_C$ ), maximum magnetic entropy change, and relative cooling power for  $\text{La}_{1.4}(\text{Sr}_{0.95}\text{Ca}_{0.05})_{1.6}\text{Mn}_2\text{O}_7$  compared with other manganites

Sample	Preparation technique	$\mu_0H(T)$	$T_C(K)$	$ \Delta S_M^{\max} (J/Kg\ K)$	$\text{RCP}_1 (J/Kg)$	Ref.
Gd	–	5	294	10.2	410	[19]
$\text{La}_{1.4}(\text{Sr}_{0.95}\text{Ca}_{0.05})_{1.6}\text{Mn}_2\text{O}_7$	Sol gel	5	248	1.71	153	This work
$\text{La}_{1.4}\text{Ca}_{1.6}\text{Mn}_2\text{O}_7$	Sol gel	4	107	0.66	101.6	[31]
$\text{La}_{1.2}\text{Ce}_{0.2}\text{Ca}_{1.6}\text{Mn}_2\text{O}_7$	Sol gel	4	100	0.56	77	[50]
$\text{La}_{1.4}\text{Sr}_{0.2}\text{Ca}_{1.4}\text{Mn}_2\text{O}_7$	Solid state	1	268	1.20	–	[28]
$\text{La}_{1.4}(\text{Sr}_{0.4}\text{Ba}_{0.6})_{1.6}\text{Mn}_2\text{O}_7$	Solid state	2	190	2.84	560	[25]

$$\Delta C_P(T, \mu_0H) = C_P(T, \mu_0H) - C_P(T, 0) = T \frac{\partial(\Delta S_M(T, \mu_0H))}{\partial T} \tag{12}$$

Figure 9 shows the  $\Delta C_P$  versus temperature under different variations of the applied magnetic field of  $\text{La}_{1.4}(\text{Sr}_{0.95}\text{Ca}_{0.05})_{1.6}\text{Mn}_2\text{O}_7$  sample calculated from the  $\Delta S_M$  data (Fig. 7) using Eq. (12). One can see that the  $\Delta C_P$  changes suddenly around  $T_C$  from positive to negative value with a positive value above  $T_C$  and a negative value below  $T_C$ . Besides, the maximum/minimum values of  $\Delta C_P$  exhibit an increasing trend with the applied magnetic field and are observed at the temperatures 261/237 K in 5 T.

Based on Landau’s theory [54] of second-order phase transition and mean-field approximation, Amaral et al. [55, 56] have investigated a successful model applicable to the MCE with the magnetoelastic contribution and electron interaction. However, this theory may not be able to explain the features near  $T_N$  because of critical fluctuations near the phase transition [57]. For this reason, we have applied this

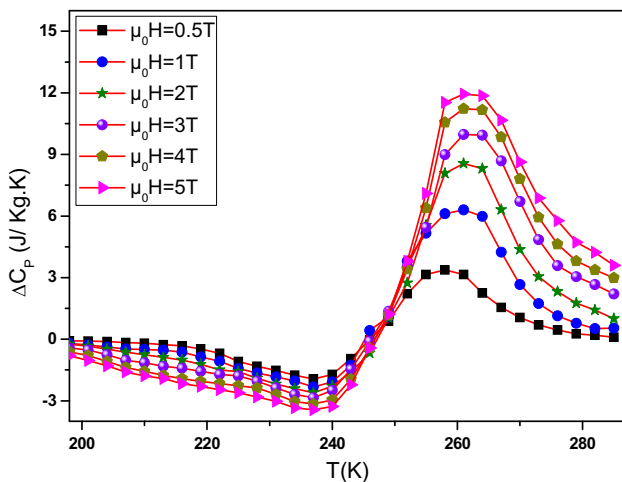


**Figure 9** Temperature dependence of ( $\Delta C_P$ ) under different variations of the applied magnetic field ( $\mu_0H$ ) for the sample.

theory around  $T_C$  and calculated the Gibb’s free energy  $G(M, T)$  which can be expressed as

$$G(M, T) = \frac{A(T)}{2}M^2 + \frac{B(T)}{4}M^4 - \mu_0HM. \tag{13}$$

According to the equilibrium condition,  $(\partial G / \partial M) = 0$ , we obtain

$$\mu_0H = A(T)M + B(T)M^3, \tag{14}$$

$$\frac{\mu_0H}{M} = A(T) + B(T)M^2, \tag{15}$$

here  $A(T)$  and  $B(T)$  are the Landau coefficients which can be determined from the plots of  $\mu_0H$  versus  $M$  at a different temperature as reported in the inset of Fig. 10. The sign of the  $B(T)$  determines the type of magnetic transition phase. If  $B(T) > 0$ , the magnetic transition is of second order, otherwise it is of first order [3, 58].

From the inset of Fig. 10, it is clear that the parameter  $A$  varies with temperature and has a

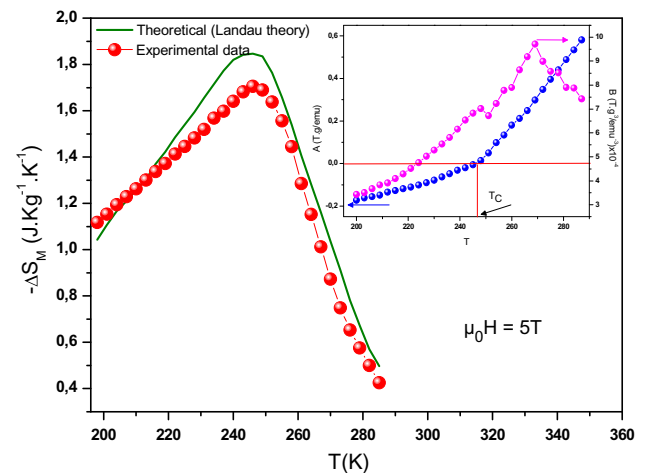


**Figure 10** Theoretical and experimental magnetic entropy changes for the sample at a magnetic field of 5 T. The inset represents the temperature dependence of Landau coefficients  $A$  and  $B$ .



minimum zero at near  $T_C$  and the value of  $B$  is positive confirming the second-order magnetic transition.

The corresponding magnetic entropy change is obtained by differentiation of the magnetic part of the free energy with respect to temperature:

$$S_M(T, \mu_0 H) = - \left( \frac{\partial G}{\partial T} \right)_H \quad (16)$$

$$= - \frac{1}{2} \frac{\partial A}{\partial T} M^2 - \frac{1}{4} \frac{\partial B}{\partial T} M^4$$

Using the  $A(T)$  and  $B(T)$  parameters, their derivative in Eq. (16), and the value of  $M(T, \mu_0 H)$ , the magnetic entropy change ( $-\Delta S_M$ ) was calculated theoretically under a magnetic field change of 5T.

Figure 10 shows the experimental and calculated results obtained by the Landau theory. There is a discrepancy between the experimental magnetic entropy change and those calculated theoretically. The analysis demonstrates that magnetoelastic coupling and electron interaction do not contribute directly to the magnetic entropy in this sample. In this case, an additional effect together with the magnetoelastic and electron interaction contributions is necessary for observed magnetic entropy data [59].

### Universal curve scaling analysis

Franco et al. [60] proposed the phenomenological universal curve which can be used as a further criterion to study the order of phase magnetic transition and was constructed by normalizing all the  $\Delta S_M(T)$  curves against their respective maximum  $\Delta S_M^{\max}$ , namely,  $\Delta S' = \Delta S_M / \Delta S_M^{\max}$  rescaling the temperature axis below and above  $T_C$  as defined in Eq. (17) with an imposed constraint that the position of two additional reference points in the curve correspond to  $\theta \pm 1$ .

$$\theta = \begin{cases} -(T - T_C) / (T_{r1} - T_C), & T \leq T_C \\ (T - T_C) / (T_{r2} - T_C), & T > T_C \end{cases} \quad (17)$$

where  $T_{r1}$  and  $T_{r2}$  are the temperatures of the two reference points that have been selected as those corresponding to  $\Delta S_M(T_{r1,2}) = 1/2 \Delta S_M^{\max}$ .

In general, for alloys with second-order phase transition, the  $\Delta S_M$  curves measured at different applied magnetic fields should collapse onto the same universal curve, while, when the scaled curves do not collapse as a single curve, the nature of the magnetic transition phase is of the first order [61].

Figure 11 shows the  $\theta$  dependence of the normalized entropy change  $\Delta S'$  for the sample. It can be clearly seen that all the experimental points in a different applied magnetic field ( $\mu_0 H = 1\text{--}5$  T) distribute on one universal curve, which confirms the occurrence of a second-order phase transition and the validity of the technique used. Materials undergoing second-order transition are good candidates for refrigerants since they have negligible hysteretic losses, while the materials undergoing first-order phase always have larger magnetic entropy change, such as gadolinium binary or ternary alloys [62]. Phan and Yu have detailed the explanation that the manganites undergoing a second-order phase transition are more active for their negligible hysteretic losses and large relative cooling capacity [19].

Recently, the magnetic field dependence of the magnetic entropy change of material with a second-order phase transition at a temperature  $T$  can be defined as [62–65]

$$\Delta S_M = a(\mu_0 H)^n, \quad (18)$$

where  $a$  is a constant and  $n$  depends on the magnetic state of the sample. It can be calculated as follows:

$$n = \frac{d \ln \Delta S_M}{d \ln(\mu_0 H)}. \quad (19)$$

By fitting the data  $\Delta S_M$  versus  $\mu_0 H$  at each temperature to Eq. (19), we determine the exponent  $n$  as

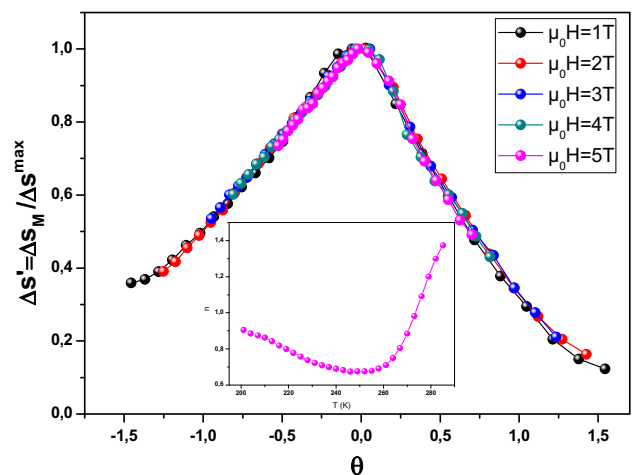


**Figure 11** Normalized entropy change dependence of the rescaled temperatures at different applied magnetic field. Inset represents the temperature dependence of the exponent  $n$  for  $\text{La}_{1.4}(\text{Sr}_{0.95}\text{Ca}_{0.05})_{1.6}\text{Mn}_2\text{O}_7$  sample.

a function of temperature as shown in the inset of Fig. 11.

It is eminent that in perovskite compounds the exponent is almost field-independent and is close to values of 1 and 2, around the transition temperature, respectively [63].

It can be clearly seen from this figure that the  $n$  exponent evolves with the temperature, it reaches 1 far below the Curie temperature and above the Curie temperature it increases with increasing temperature and the value approach 2 due to the Curie–Weiss law reflects an increasing sensitivity of the magnetic entropy to apply magnetic field in this temperature range. The minimum  $n$  value around  $T_C$  equal to 0.68 is close to the  $2/3$  value predicted by Oesterreicher and Parker [66]. It was reported that the  $n$  exponent has a significant dependence on the size of manganites and exhibits an increasing trend with reducing their size [63].

### Critical behavior

In order to understand the exact nature of the second-order magnetic phase transition occurring around the Curie point, we used Arrott plots to determine the Curie temperature and the critical exponents in the vicinity of the phase transition temperature. The exponent's  $\beta$  (associated with the spontaneous magnetization  $M_S(T) = \lim_{H \rightarrow 0} M$  just below  $T_C$ ),  $\delta$  (associated with the critical magnetization isotherm at  $T_C$ ), and  $\gamma$  (relevant to the initial magnetic susceptibility  $\chi_0, \chi_0^{-1}(T) = \lim_{H \rightarrow 0} (\mu_0 H/M)$  just above  $T_C$ ) are given in the following relation [67–69]:

$$M_S(T, 0) = M_0(-\varepsilon)^\beta; \quad T < T_C, \quad \varepsilon < 0. \quad (20)$$

The exponent  $\gamma$  describes the temperature dependence of the zero-field susceptibility and is defined as

$$\chi_0^{-1}(T) = \left(\frac{h_0}{M_0}\right) \varepsilon^\gamma; \quad T > T_C, \quad \varepsilon = 0. \quad (21)$$

The exponent  $\delta$  describes the field dependence of the magnetization at the Curie temperature,  $T_C$ :

$$M = DH^{1/\delta}; \quad T = T_C, \quad (22)$$

here  $\varepsilon = (T - T_C)/T_C$  is the reduced temperature. The critical exponents  $\beta, \gamma,$  and  $\delta,$  as well as the critical amplitudes  $M_0, h_0,$  and  $D$  exhibit universal behavior near the phase transition point. There are several universality classes with sets of critical indices that depend on the spin and the special

dimensionality. As we know, for a first-order ferromagnetic phase transition, the critical exponents are impossible to define because the applied magnetic field depends on the temperature  $T_C(\mu_0 H)$  [70].

From the Arrott plot  $M^2$  versus  $\mu_0 H/M$  in Fig. 6, the reliable values of the inverse initial susceptibility  $\chi_0^{-1}(T)$  and the spontaneous magnetization  $M_S(T)$  have been determined by the linear extrapolation of the high-field region toward the intercepts with both axes ( $\mu_0 H/M$ ) and  $M^2$  below and above  $T_C$ , respectively.

These results are shown in Fig. 12a as functions of temperature. By fitting these plots using Eqs. (20) and (21), we get to the values of  $\beta = 0.594, \gamma = 1.048,$  and  $T_C = 248$  K.

Moreover, in order to determine the parameters  $T_C, \beta$  and  $\gamma$  more precisely, we also analyzed  $M_S(T, 0)$  and  $\chi_0^{-1}(T)$  values using the Kouvel-Fisher (KF) method [71, 72]:

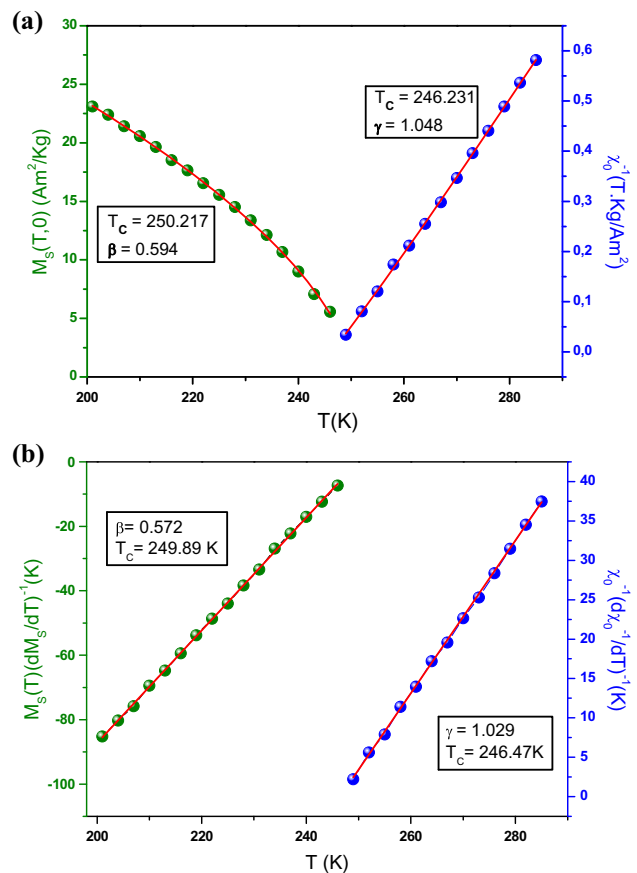


**Figure 12** a Temperature dependence of the spontaneous magnetization  $M_S(T, 0)$  and the inverse initial susceptibility  $\chi_0^{-1}$  along with the fitting curves (solid lines) based on the power laws. b Kouvel-Fisher plots for  $M_S(T)(dM_S/dT)^{-1}$  and  $\chi_0^{-1}(T)(d\chi_0^{-1}/dT)^{-1}$ .

$$M_S(T)/(dM_S(T)/dT) = (T - T_C)/\beta, \quad (23)$$

$$\chi_0^{-1}(T)/(d\chi_0^{-1}(T)/dT) = (T - T_C)/\gamma. \quad (24)$$

According to these equations, the parameters  $M_S(T)[dM_S(T)/dT]^{-1}$  and  $\chi_0^{-1}(T)[d\chi_0^{-1}(T)/dT]^{-1}$  are plotted versus  $T$  in Fig. 12b and should yield straight lines with slopes of  $1/\beta$  and  $1/\gamma$ , respectively, and the value of  $T_C$  is obtained from intercepts on the temperature axis.

The linear fitting to the plots following the KF method gives  $\beta = 0.572$ ,  $\gamma = 1.029$ , and  $T_C = 248$  K.

Obviously, the values of  $\beta$ ,  $\gamma$ , and  $T_C$  obtained by the KF method are in good agreement with that using the Arrott plot  $M^2$  versus  $\mu_0 H/M$ .

Further, the critical exponent  $\delta$  has also been determined directly by plotting the critical isotherm at  $T_C$ . In Fig. 13, the  $M$  versus  $\mu_0 H$  curve are plotted at 248 K, which is close to the  $T_C$ . The inset presents the  $M$  versus  $\mu_0 H$  plot logarithmic scale. According to Eq. (22), in the high-field region of the data, the solid straight line with the slope ( $1/\delta$ ) is the fitting result. This gives the third critical exponent  $\delta = 2.549$ .

According to statistical theory, these three critical exponents are related according to the Widom scaling relationship [72–74] given by

$$\delta = 1 + \frac{\gamma}{\beta}. \quad (25)$$

Using this scaling relation and the critical exponents  $\beta$  and  $\gamma$ , obtained above from the Arrott plot  $M^2$  versus  $\mu_0 H/M$  and KF method, we obtain  $\delta = 2.764$

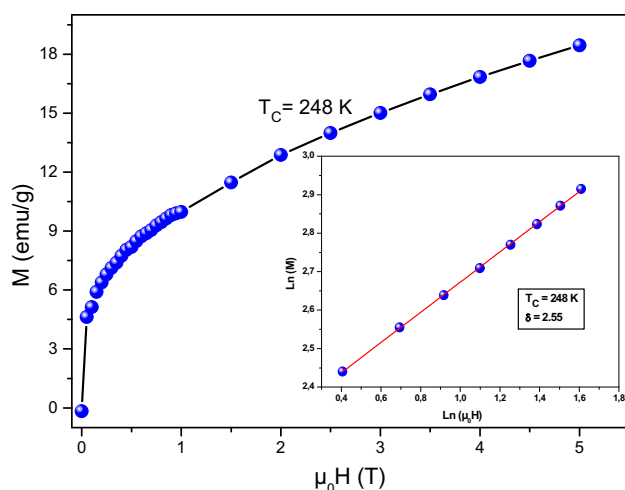


**Figure 13** Critical isotherms of  $M$  versus  $\mu_0 H$  at  $T_C$ . The inset shows the same plot in log–log scale and the straight line is the linear fit following Eq. (22).

and 2.798, respectively. These values are in good agreement and close to those obtained from the critical isotherms at  $T_C$ . Thus, the critical exponents, found in this work, obey the Widom scaling relation remarkably well. Moreover, we can note that these values for the critical exponents are close to the mean-field values ( $\beta = 0.5$ ,  $\gamma = 1$  and  $\delta = 3$ ) [75].

In the critical region, to further investigate the reliability of the calculated exponents values  $\beta$ ,  $\gamma$ , and  $\delta$  and the validity of the Widom scaling relation, the magnetic equation of state can be written as [76]

$$M(\mu_0 H, \varepsilon) = \varepsilon^\beta f_\pm(\mu_0 H/\varepsilon^{\beta+\gamma}), \quad (26)$$

where  $f_+$  for the paramagnetic state for  $T > T_C$  and  $f_-$  for the ferromagnetic state for  $T < T_C$  are regular analytic functions and the values of  $\beta$  and  $\gamma$  were obtained from KF method. Equation (26) implies that the scaled  $M/|\varepsilon^\beta|$  plotted as a function of  $\mu_0 H/|\varepsilon|^{\beta+\gamma}$  in Fig. 14 yields in the vicinity of  $T_C$  two distinct curves, one for temperatures  $T < T_C$  and the other for temperatures  $T > T_C$ . The scaled data proved that the critical exponents and  $T_C$  obtained are in good accordance with the scaling hypothesis.

The inset of Fig. 14 shows the same plots in log–log scale. It is clearly observed, at higher fields, that these two curves at  $T < T_C$  and  $T > T_C$  coincided. However, the scaling becomes poor toward lower fields. This behavior is due to the Arrott plot which deviates from linearity at low field, due to the mutually misaligned magnetic domains.

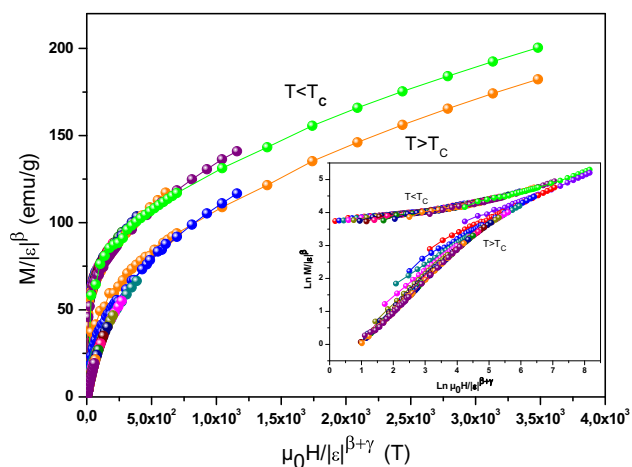


**Figure 14** Scaling plots for compound below and above  $T_C$ , using the  $\beta$  and  $\gamma$  exponents determined from the KF method, indicating two universal curves. The insets show the same plots on a log–log scale.

Based on the renormalization group analysis of systems, performed by Fisher et al. [72], the universality class of the magnetic phase transition depends on the range of exchange interaction  $J(r) = 1/r^{d+\sigma}$ , where  $r$  is the distance between the interacting spins,  $d$  is the dimension of the system, and  $\sigma > 0$  is the range of the interaction.

For three-dimensional materials ( $d = 3$ ), the relation becomes  $J(r) = r^{-3-\sigma}$ . It has been argued that, if  $J(r)$  decreases faster than  $r^{-5}$  ( $\sigma$  greater than 2), the Heisenberg exponents ( $\beta = 0.365$ ,  $\gamma = 1.336$  and  $\delta = 4.8$ ) is valid for a 3D-isotropic ferromagnet. However, if  $J(r)$  decreases slower than  $r^{-4.5}$  ( $\sigma$  is less than  $3/2$ ), the mean-field model ( $\beta = 0.5$ ,  $\gamma = 1.0$  and  $\delta = 3.0$ ) is satisfactory. In the intermediate range with  $3/2 \leq \sigma \leq 2$ , the exponents belong to different universality class which depends upon  $\sigma$  (such as the tricritical mean-field theory and 3D Ising model). In general way, the evolution of the critical exponents tends toward the values of the mean-field theory.

In the following section, we will use the obtained magnetic entropy change to study the spontaneous magnetization in this sample. According to the mean-field theory, the magnetic entropy can be expressed as a function of magnetization [77, 78]:

$$S(\sigma) = -Nk_B \left[ \ln(2J + 1) - \ln \frac{\sinh\left(\frac{2J+1}{2J} B_J^{-1}(\sigma)\right)}{\sinh\left(\frac{1}{2J} B_J^{-1}(\sigma)\right)} + B_J^{-1}(\sigma)\sigma \right], \tag{27}$$

where  $N$  is the number of spins,  $k_B$  is Boltzmann constant,  $J$  is the spin value,  $B_J$  is the Brillouin function for a given  $J$  value, and  $\sigma$  the reduced magnetization.

$$(\sigma = (M/gJN)\mu_B).$$

For small  $M$  values, Eq. (27) can be performed using a power expansion, and the magnetic entropy  $\Delta S_M$  is proportional to  $M^2$ :

$$-S(\sigma) = \frac{3}{2J+1} Nk_B \sigma^2 + o(\sigma^4). \tag{28}$$

Furthermore, in the ferromagnetic state ( $T < T_C$ ), the material produces a spontaneous magnetization  $M_S$  and the  $\sigma = 0$  state is never attained. If we only consider the first term of the expansion of Eq. (28), this corresponds to

$$-S(\sigma) = \frac{3}{2J+1} Nk_B (\sigma^2 + \sigma_S^2). \tag{29}$$

Equation (29) indicates that the  $-\Delta S_M$  versus  $M^2$  curve shows a linear variation. We plotted this curve based on the obtained magnetic entropy change and magnetization. As shown in Fig. 15, all curves at different temperatures (224–245 K) obey the same regularity and a clear linear dependence with an approximately constant slope (0.0034), indicating that it is appropriate for us to analyze the current experimental results with the mean-field theory.

Therefore, the spontaneous magnetization  $M_S$  of material can be estimated from the linear fits of  $-\Delta S_M$  versus  $M^2$  curve at different temperatures, which is shown in Fig. 16.

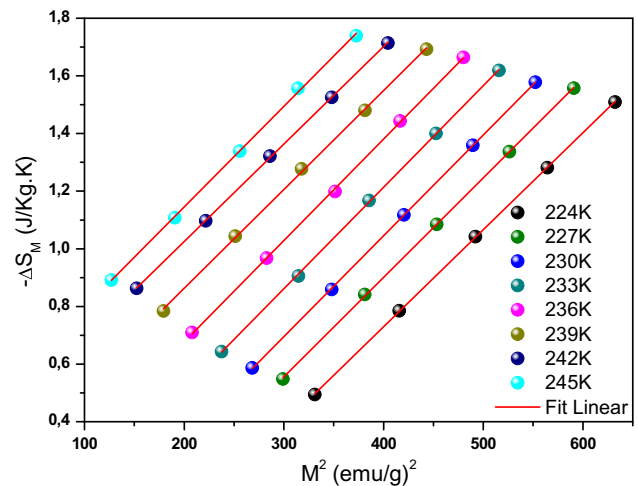


**Figure 15** Isothermal ( $-\Delta S_M$ ) versus  $M^2$  curves. The solid lines are linear fits to data.

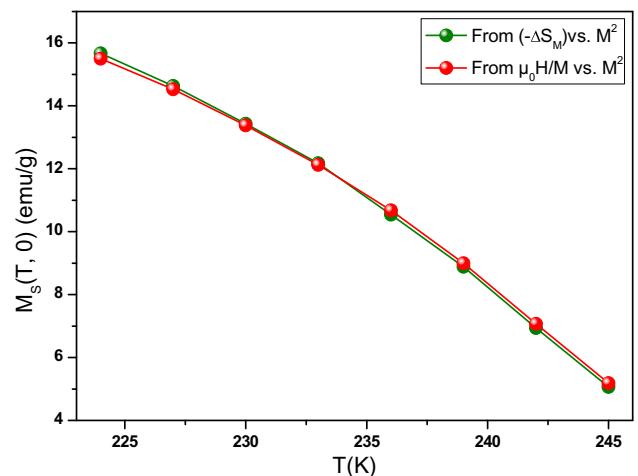


**Figure 16** Spontaneous magnetization of  $\text{La}_{1.4}(\text{Sr}_{0.95}\text{Ca}_{0.05})_{1.6}\text{Mn}_2\text{O}_7$  deduced from the extrapolation of the isothermal  $-\Delta S_M$  versus  $M^2$  curves and from the mean-field results.

We can see that when the temperature decreases, the spontaneous magnetization becomes larger and larger, suggesting that the compound is approaching a spin ordering state, at lower temperature.

For comparison, the spontaneous magnetization can be also determined from the experimental Arrott plot (namely,  $M^2$  versus  $H/M$ ), as shown in Fig. 12a.

Obviously, the excellent agreement between the two methods is obtained, confirming that the present magnetic system should be close to mean-field theory.

## Conclusion

In summary, we have prepared  $\text{La}_{1.4}(\text{Sr}_{0.95}\text{Ca}_{0.05})_{1.6}\text{Mn}_2\text{O}_7$  polycrystalline sample by sol-gel route. Magnetic properties, magnetocaloric effect, and the critical properties have been studied in detail.

The variation of the magnetization versus temperature, under an applied magnetic field of 0.05 T, revealed that the compound shows ferromagnetic behavior with a Curie temperature of 248 K and a Neel transition at  $T_N = 170$  K.

Besides the universal curves confirmed that the magnetic phase transition is of the second order in nature. Then, the maximum entropy change of  $1.71 \text{ J kg}^{-1} \text{ K}^{-1}$  and  $\text{RCP} = 153.77 \text{ J/kg}$  were observed at 5 T magnetic field. The estimated critical exponents confirm that the experimental data agree well with the mean-field model. The methodology based on the analysis of the magnetic entropy change ( $-\Delta S_M$ ) versus  $M^2$ , compared with the classical extrapolation of the Arrott curves ( $\mu_0 H/M$  versus  $M^2$ ), confirm that the magnetic entropy change is a valid method to determine the spontaneous magnetization of  $\text{La}_{1.4}(\text{Sr}_{0.95}\text{Ca}_{0.05})_{1.6}\text{Mn}_2\text{O}_7$  system and eventually of other compounds.

## Compliance with ethical standards

**Conflict of interest** The authors (Arwa. Belkahla, K. Cherif, J. Dhahri, E. K. Hlil) declare that they have no conflict of interest.

## References

- [1] Gschneidner KA Jr, Pecharsky VK, Tsokol AO (2005) Recent developments in magnetocaloric materials. *Rep Prog Phys* 68:1479–1539
- [2] Zimm C, Jastrab A, Sternberg A, Pecharsky V, Gschneidner KA Jr, Osborne M, Anderson I (1998) Description and performance of a near-room temperature magnetic refrigerator. *Adv Cryog Eng* 43:1759–1766
- [3] Pecharsky VK, Gschneidner KA (1999) Magnetocaloric effect and magnetic refrigeration. *J Magn Magn Mater* 200:44–46
- [4] Bruck E (2005) Developments in magnetocaloric refrigeration. *J Phys D: Appl Phys* 38:R381–R391
- [5] Das S, Dey TK (2007) Magnetic entropy change in polycrystalline  $\text{La}_{1-x}\text{K}_x\text{MnO}_3$  perovskites. *J Alloys Compd* 440(1–2):30–35
- [6] Sheik MM, Sudheendra L, Rao CNR (2004) Magnetic properties of  $\text{La}_{0.5-x}\text{Ln}_x\text{Sr}_{0.5}\text{MnO}_3$  ( $\text{Ln} = \text{Pr, Nd, Gd and Y}$ ). *J Solid State Chem* 177(10):3633–3639
- [7] Phan MH, Yu SC (2007) Review of the magnetocaloric effect in manganite materials. *J Magn Magn Mater* 308(2):325–340
- [8] Amano ME, Betancourt I, Sánchez Llamazares JL, Huerta L, Sánchez-Valdés CF (2014) Mixed-valence  $\text{La}_{0.80}(\text{Ag}_{1-x}\text{Sr}_x)_{0.20}\text{MnO}_3$  manganites with magnetocaloric effect. *J Mater Sci* 49:633–641. doi:10.1007/s10853-013-7743-5
- [9] Phan MH, Tian SB, Yu SC, Ulyanov AN (2003) Magnetic and magnetocaloric properties of  $\text{La}_{0.7}\text{Ca}_{0.3-x}\text{Ba}_x\text{MnO}_3$  compounds. *J Magn Magn Mater* 256(1–3):306–310
- [10] Tian SB, Phan MH, Yu SC, HwiHur N (2003) Magnetocaloric effect in a  $\text{La}_{0.7}\text{Ca}_{0.3}\text{MnO}_3$  single crystal. *Phys B* 327(2–4):221–224
- [11] Shao MJ, Cao SX, Wang YB, Yuan SJ, Kang BJ, Zhang JC (2012) Large magnetocaloric effect in  $\text{HoFeO}_3$  single crystal. *Solid State Commun* 152:947–950
- [12] Ben Jemaa F, Mahmood S, Ellouze M, Hlil EK, Halouani F (2015) Structural, magnetic, and magnetocaloric studies of  $\text{La}_{0.67}\text{Ba}_{0.22}\text{Sr}_{0.11}\text{Mn}_{1-x}\text{Co}_x\text{O}_3$  manganites. *J Mater Sci* 50:620–633. doi:10.1007/s10854-015-3085-1
- [13] Sebald G, Pruvost S, Seveyrat L, Lebrun L, Guyomar D, Guiffard B (2007) Electrocaloric properties of high dielectric constant ferroelectric ceramics. *J Eur Ceram Soc* 27:4021
- [14] Pamir Alpay S, Mantese Joseph, Trolier-McKinstry Susan, Zhang Qiming, Whatmore Roger W (2014) Next-generation electrocaloric and pyroelectric materials for solid-state electrothermal energy interconversion. *MRS Bull* 39:1099–1108
- [15] Fawcett ID, Kim E, Greenblatt M, Croft M, Bendersky LA (2000) Properties of the electron-doped layered manganites  $\text{La}_{2-2x}\text{Ca}_{1+2x}\text{Mn}_2\text{O}_7$  ( $0.6 \leq x \leq 1.0$ ). *Phys Rev B* 62:6485–6495
- [16] Li JQ, Jin CQ, Zhao HB (2001) Structural and physical properties of double-layered manganites  $\text{La}_{2-2x}\text{Ca}_{1+2x}\text{Mn}_2\text{O}_7$  with  $0.5 \leq x \leq 1.0$ . *Phys Rev B* 64:020405(R)
- [17] Allodi G, Bimbi M, De Renzi R, Baumann C, Apostu M, Suryanarayanan R, Revcovschi A (2008) Magnetic order

- in the double-layer manganites  $(\text{La}_{1-x}\text{Pr}_x)_{1.2}\text{Sr}_{1.8}\text{Mn}_2\text{O}_7$ : intrinsic properties and role of intergrowth. *Phys Rev B* 78:064420–064430
- [18] Ramirez AP (1997) Colossal magnetoresistance. *J Phys: Condens Matter* 9:8171–8199
- [19] Kumaresavanji M, Saitovitch EMB, Araujo JP, Fontes MB (2013) Pressure-enhanced ferromagnetism and metallicity in  $\text{La}_{1.24}\text{Sr}_{1.76}\text{Mn}_2\text{O}_7$  bilayered manganite system. *J Mater Sci* 48:1324–1329. doi:10.1007/s10853-012-6877-1
- [20] Zener C (1951) Interaction between the d-shells in the transition metals. II. Ferromagnetic compounds of manganese with perovskite structure. *Phys Rev* 82:403
- [21] Gor'kov LP, Kresin VZ (2004) Mixed-valence manganites: fundamentals and main properties. *Phys Rep* 400:149–208
- [22] Millis AJ, Littlewood PB, Shraiman BI (1995) Double exchange alone does not explain the resistivity of  $\text{La}_{1-x}\text{Sr}_x\text{MnO}_3$ . *Phys Rev Lett* 74:144
- [23] Han L, Chen C (2010) Magnetocaloric and colossal magnetoresistance effect in layered perovskite  $\text{La}_{1.4}\text{Sr}_{1.6}\text{Mn}_2\text{O}_7$ . *J Mater Sci Technol* 26:234–236. doi:10.1016/j.jssc.2003.12.037
- [24] Wang A, Cao G, Liu Y, Long Y, Li Y, Feng Z, Ross JH (2005) Magnetic entropy change of the layered perovskites  $\text{La}_{2-2x}\text{Sr}_{1+2x}\text{Mn}_2\text{O}_7$ . *J Appl Phys* 97:103906
- [25] Cherif K, Zemni S, Dhahri J, Oumezzine M, Said M, Vincent H (2007) Magnetocaloric effect in layered perovskite manganese oxide  $\text{La}_{1.4}(\text{Sr}_{1-x}\text{Ba}_x)_{1.6}\text{Mn}_2\text{O}_7$  ( $0 \leq x \leq 0.6$ ) bulk materials. *J Alloys Compd* 432:30–33
- [26] Zhu H, Song H, Zhang YH (2002) Magnetocaloric effect in layered perovskite manganese oxide  $\text{La}_{1.4}\text{Ca}_{1.6}\text{Mn}_2\text{O}_7$ . *Appl Phys Lett* 81(1):3416–3419
- [27] Tetean R, Himcinschi C, Burzo E (2008) Magnetic properties and magnetocaloric effect in  $\text{La}_{1.4-x}\text{R}_x\text{Ca}_{1.6}\text{Mn}_2\text{O}_7$  compounds with R. *J Optoelectron Adv Mater* 10:849–852
- [28] Zhao X, Chen W, Zong Y, Diao SL, Yan XJ, Zhu MG (2009) Structure, magnetic and magnetocaloric properties in  $\text{La}_{1.4}\text{Sr}_{1.6-x}\text{Ca}_x\text{Mn}_2\text{O}_7$  perovskite compounds. *J Alloys Compd* 469:61–65
- [29] Arwa Belkahla K, Cherif JD, Hlil EK (2015) Structural and optical properties of the Ruddlesden-Popper  $\text{La}_{1.4}(\text{Sr}_{0.95}\text{Ca}_{0.05})_{1.6}\text{Mn}_2\text{O}_7$  sample prepared by a sol-gel method. *J Super Nov Magn* 29:19–27
- [30] Ma Y, Dong QY, Ke YJ, Wu YD, Zhang XQ, Wang LC, Shen BG, Sun JR, Cheng ZH (2015) Eu doping-induced enhancement of magnetocaloric effect in manganite  $\text{La}_{1.4}\text{Ca}_{1.6}\text{Mn}_2\text{O}_7$ . *Solid State Commun* 208:25–28
- [31] Dudric R, Goga F, Mican S, Tetean R (2013) Effects of substitution of PR, Nd, and Sm for La on the magnetic properties and magnetocaloric effect of  $\text{La}_{1.4}\text{Ca}_{1.6}\text{Mn}_2\text{O}_7$ . *J Alloy Compd* 553:129–134
- [32] Yang J, Song WH, Ma YQ, Zhang RL, Zhao BC, Sheng ZG, Zheng GH, Dai JM, Sun YP (2004) Structural, magnetic, and transport properties in the Pr-doped manganites  $\text{La}_{0.9-x}\text{Pr}_x\text{Te}_{0.1}\text{MnO}_3$  ( $0 \leq x \leq 0.9$ ). *Phys Rev B* 70:144421
- [33] Dho J, Kim WS, Hur XH (2002) Reentrant spin glass behavior in Cr-doped perovskite manganite. *Phys Rev Lett* 89:027202(1–4)
- [34] Shen CH, Liu RS, Hu SF, Huang CY, Sheu HS (1999) Structural, electrical and magnetic properties of two-dimensional  $\text{La}_{1.2}(\text{Sr}_{1.8-x}\text{Ca}_x)\text{Mn}_2\text{O}_7$  manganites. *J Appl Phys* 86:2178–2184
- [35] Philipp JB, Klein J, Recher C, Walther T, Mader W, Schmid M, Suryanarayanan R, Alff L, Gross R (2002) Microstructure and magnetoresistance of epitaxial films of the layered perovskite  $\text{La}_{2-2x}\text{Sr}_{1+2x}\text{Mn}_2\text{O}_7$  ( $x = 0.3$  and  $0.4$ ). *Phys Rev B* 65:184411-1
- [36] Chatterji T, Koza MM, Demmel F, Schmidt W, Aman U, Schneider R, Dhalenne G, Suryanarayanan R, Revcolevschi A (2006) Coexistence of ferromagnetic and antiferromagnetic spin correlations in  $\text{La}_{1.2}\text{Sr}_{1.8}\text{Mn}_2\text{O}_7$ . *Phys Rev B* 73:10449(1–6)
- [37] Zhou TJ, Yu Z, Zhong W, Xu XN, Zhang HH, Du YW (1999) Larger magnetocaloric effect in two-layered  $\text{La}_{1.6}\text{Ca}_{1.4}\text{Mn}_2\text{O}_7$  polycrystal. *J Appl Phys* 85:7975–7977
- [38] Liniers M, Flores J, Bermejo FJ, Gonzalez JM, Vicent JL, Tejada J (1989) Systematic study of the temperature dependence of the saturation magnetization in Fe, Fe-Ni and Co-based amorphous alloys. *IEEE Trans Magn* 25:3363
- [39] Padmanabhan B, Elizabeth S, Bhat HL, Rosler S, Dorr K, Muller KH (2006) Crystal growth, transport and magnetic properties of rare-earth manganite  $\text{Pr}_{1-x}\text{Pb}_x\text{MnO}_3$ . *J Magn Magn Mater* 307:288–294
- [40] Ghosh N, Elizabeth S, Bhat HL, Rossler UK, Nenkov K, Rossler S, Dorr K, Muller K-H (2004) Effect of rare-earth-site cations on the physical properties of  $\text{La}_{0.7-y}\text{Nd}_y\text{Pb}_{0.3}\text{MnO}_3$  single crystals. *Phys Rev B* 70:184436
- [41] Kittel C (1993) Quantum theory of solids. Wiley, New York
- [42] Oubla M, Lamire M, Lassri H, Hlil EK (2013) Structural and magnetic properties of layered perovskite manganite  $\text{LaCaBiMn}_2\text{O}_7$ . MATEC Web of Conference, vol 5, p 04040
- [43] Katsuki A, Wollfarth EP (1966) Spin waves and their stability in metals. *Proc R Soc A* 295:182–191
- [44] Banerjee BK (1964) On a generalized approach to first and second order magnetic transitions. *Phys Lett* 12:16–17
- [45] Hashimoto T, Numasawa T, Shino M, Okada T (1981) Magnetic refrigeration in the temperature range from 10 K to room temperature: the ferromagnetic refrigerants. *Cryogenics* 21:647–653

- [46] Biswas A, Samanta T, Babarjee S, Das I (2009) Inverse magnetocaloric effect in polycrystalline  $\text{La}_{0.125}\text{Ca}_{0.875}\text{MnO}_3$ . *J Phys: Condens Matter* 21:506005(1-3)
- [47] Ben Amor N, Bejar M, Hussein M, Dhahri E, Valente MA, Hlil EK (2013) Magnetocaloric effect in the vicinity of second order antiferromagnetic transition of  $\text{Er}_2\text{Mn}_2\text{O}_7$  compound at different applied magnetic field. *J Alloys Compd* 563:28–32
- [48] Zhou KW, Zhuang YH, Li JQ, Deng JQ, Zhu QM (2006) Magnetocaloric effects in  $(\text{Gd}_{1-x}\text{Tb}_x)\text{Co}_2$ . *Solid State Commun* 137:275–277
- [49] Giri SK, Dasgupta P, Poddar A, Sahoo RC, Paladhi D, Nath TK (2015) Strain modulated large magnetocaloric effect in  $\text{Sm}_{0.55}\text{Sr}_{0.45}\text{MnO}_3$  epitaxial films. *J Appl Phys Lett* 106:023507(1-5)
- [50] Dudric R, Goga F, Neumann M, Mican S, Tetean R (2012) Magnetic properties and magnetocaloric effect in  $\text{La}_{1.4-x}\text{Ce}_x\text{Ca}_{1.6}\text{Mn}_2\text{O}_7$  perovskites synthesized by sol-gel method. *J Mater Sci* 47:3125–3130. doi:10.1007/s10853-011-6146-8
- [51] Rostamnejadi A, Venkatesan M, Kameli P, Salamati H, Coey JMD (2011) Magnetocaloric effect in  $\text{La}_{0.67}\text{Sr}_{0.33}\text{MnO}_3$  manganite above room temperature. *J Magn Magn Mater* 323:2214–2218
- [52] Yang H, Zhu YH, Xian T, Jiang JL (2013) Synthesis and magnetocaloric properties of  $\text{La}_{0.7}\text{Ca}_{0.3}\text{MnO}_3$  nanoparticles with different sizes. *J Alloys Compd* 555:150–155
- [53] Zhong W, Chen W, Ding WP, Zhang N, Hu A, Du YW, Yan QJ (1998) Structure, composition and magnetocaloric properties in polycrystalline  $\text{La}_{1-x}\text{A}_x\text{MnO}_{3+\delta}$  ( $\text{A} = \text{Na}, \text{K}$ ). *Eur Phys J B* 3:169
- [54] Landau LD, Lifshitz EM (1958) *Statistical physics*. Pergamon, New York
- [55] Amaral JS, Reis MS, Amaral VS, Mendonça TM, Araujo JP, Sa MA, Tavares PB, Vieira JM (2005) Magnetocaloric effect in Er- and Eu-substituted ferromagnetic La-Sr manganites. *J Magn Magn Mater* 290–291:686–689
- [56] Amaral VS, Amaral JS (2004) Magnetoelastic coupling influence on the magnetocaloric effect in ferromagnetic materials. *J Magn Magn Mater* 272–276:2104–2105
- [57] Levy LP (2000) *Magnetism and superconductivity*. Springer, Berlin
- [58] Bebenin NG, Zainullina RI, Ustinov VV, Mukovskii Ya M (2012) Effect of inhomogeneity on magnetic, magnetocaloric, and magnetotransport properties of  $\text{La}_{0.6}\text{Pr}_{0.1}\text{Ca}_{0.3}\text{MnO}_3$  single crystal. *J Magn Magn Mater* 324:1112–1116
- [59] Cherif R, Hlil EK, Ellouze M, Elhalouani F, Obbade S (2014) Study of magnetic and magnetocaloric properties of  $\text{La}_{0.6}\text{Pr}_{0.1}\text{Ba}_{0.3}\text{MnO}_3$  and  $\text{La}_{0.6}\text{Pr}_{0.1}\text{Ba}_{0.3}\text{Mn}_{0.9}\text{Fe}_{0.1}\text{O}_3$  perovskite-type manganese oxides. *J Mater Sci* 49:8244–8251. doi:10.1007/s10853-014-8533-4
- [60] Franco V, Blazquez JS, Conde A (2008) Influence of Ge addition on the magnetocaloric effect of a Co-containing nanoperm-type alloy. *J Appl Phys* 103:07B316–07B321
- [61] Bonilla CM, Albillos JH, Bartolome F, Garcia LM, Borderias MP, Franco V (2010) Universal behavior for magnetic entropy change in magnetocaloric materials: an analysis on the nature of phase transitions. *Phys Rev B* 81:224424–224431
- [62] Pecharsky AO, Pecharsky VK, Gschneidner KA (2003) The giant magnetocaloric effect of optimally prepared  $\text{Gd}_5\text{Si}_2\text{Ge}_2$ . *J Appl Phys* 93:4722–4728
- [63] Pekala M (2010) Magnetic field dependence of magnetic entropy change in nanocrystalline and polycrystalline manganites  $\text{La}_{1-x}\text{M}_x\text{MnO}_3$  ( $\text{M} = \text{Ca}, \text{Sr}$ ). *J Appl Phys* 108:113913–1139134
- [64] Dong QY, Zhang HW, Sun JR, Shen BG, Franco V (2008) A phenomenological fitting curve for the magnetocaloric effect of materials with a second-order phase transition. *J Appl Phys* 103:116101
- [65] Franco V, Conde CF, Conde A, Kiss LF (2007) Enhanced magnetocaloric response in Cr/Mo containing nanoperm-type amorphous alloys. *Appl Phys Lett* 90:052509
- [66] Oesterreicher H, Parker FT (1984) Magnetic cooling near Curie temperatures above 300K. *J Appl Phys* 55:4334
- [67] Moutis N, Panagiotopoulos I, Pissas M, Niarchos D (1999) Structural and magnetic properties of  $\text{La}_{0.67}(\text{Ba}_x\text{Ca}_{1-x})_{0.33}\text{MnO}_3$  perovskites ( $0 < x < 1$ ). *Phys Rev B* 59:1129–1138
- [68] Yang J, Lee YP (2007) Critical behavior in Ti-doped manganites  $\text{LaMn}_{1-x}\text{Ti}_x\text{O}_3$  ( $0.05 \leq x \leq 0.2$ ). *Appl Phys Lett* 91:142512
- [69] Xuebin Z, Shixue D (2010) Crossover of critical behavior in  $\text{La}_{0.7}\text{Ca}_{0.3}\text{Mn}_{1-x}\text{Ti}_x\text{O}_3$ . *J Magn Magn Mater* 322:242–256
- [70] Kim D, Revaz B, Zink BL, Hellman F, Rhyne JJ, Mitchell JF (2002) Tricritical point and the doping dependence of the order of the ferromagnetic phase transitions of  $\text{La}_{1-x}\text{Ca}_x\text{MnO}_3$ . *Phys Rev Lett* 89:227202–227205
- [71] Kouvel JS, Fisher ME (1964) Detailed magnetic behavior of nickel near its Curie point. *Phys Rev* 136:A1626–A1632
- [72] Fisher ME, Ma SK, Nickel BG (1972) Critical exponents for long-range interactions. *Phys Rev Lett* 29:917–920
- [73] Widom B (1965) Equation of state in the neighborhood of the critical point. *J Chem Phys* 43:3898–3905
- [74] Shin HS, Lee JE, Nam YS, Ju HL, Park CW (2001) First-order-like magnetic transition in manganite oxide  $\text{La}_{0.7}\text{Ca}_{0.3}\text{MnO}_3$ . *Solid State Commun* 118:377
- [75] Franco V, Conde A, Romero EJM, Blazquez JS (2008) A universal curve for the magnetocaloric effect: an analysis

- based on scaling relations. *J Phys: Condens Matter* 20:285207
- [76] Eugene Stanley H (1971) *Introduction to phase transitions and critical phenomena (International Series of Monographs on Physics)*. Oxford University Press, New York
- [77] Tishin AM, Spichin YI (2003) *The magnetocaloric effect and its applications*. IOP Publishing, London
- [78] Amaral JS, Silva NJO, Amaral VS (2010) Estimating spontaneous magnetization from a mean field analysis of the magnetic entropy change. *J Magn Magn Mater* 322:1569